ADVANCED FUNCTIONAL MATERIALS
www.afm-journal.de

Bright and Photostable Organic Fluorescent Dots with Aggregation-Induced Emission Characteristics for Noninvasive Long-Term Cell Imaging

Wei Qin, Kai Li, Guangxue Feng, Min Li, Zhiyong Yang, Bin Liu, and Ben Zhong Tang**

Efficient long-term cell tracing in a noninvasive and real-time manner is of great importance to understand genesis, development, invasion, and metastasis of cancerous cells. Cell penetrating organic dots with aggregation-induced emission (AIE) characteristics are successfully developed as long-term cell trackers. The AIE dots enjoy the advantages of high emission efficiency, large Stokes shift, good biocompatibility, and high photostability, which ensure their good performance in long-term non-invasive in vitro cell tracing. Moreover, it is the first report that AIE dots exhibit certain permeability to cellular nucleus, making them attractive potential candidates for nucleus imaging. The AIE dots display superior performance compared to their counterparts of inorganic quantum dots, opening a new avenue in the development of fluorescent probes for monitoring biological processes.

1. Introduction

Fluorescence imaging as a highly sensitive and non-invasive technology,[1] offers researchers a very useful tool to locate and monitor biological targets within complex and dynamic intracellular environments.[2] Direct visualization of genesis, development, invasion, and metastasis of cancerous cells are ideal for medical diagnostics and therapeutics of cancerization at the early stage. Green fluorescent protein (GFP) and its family have been adopted for genetic cell tagging to achieve long-term cell tracing.[3] Unfortunately, some inherent drawbacks of GFP are unavoidable, such as the susceptibility to enzyme degradation, small Stokes shifts, and poor photostability.[4] Moreover, transfection of fluorescent protein is a tedious and time-consuming process, which often yields low labeling efficiency.[5] Recent studies also reveal that fluorescent protein transfection can interfere with normal cell functions, which hampers practical applications of the GFP-based probes.[6]

Besides GFP, inorganic semiconductor quantum dots (QDs) are widely used as fluorescent probes for direct cell labeling,[7] which have shown bright emission and high photobleaching threshold under imaging conditions.[8] Unfortunately, the commonly used QDs (e.g., CdSe and CdTe) contain heavy metal elements, which are highly cytotoxic in oxidative environments.[9] In addition, QDs are liable to aggregate in cells[10] and show unstable fluorescence signals.[8,11] These detrimental effects hinder their future application in clinical settings.

Organic fluorophore-loaded nanoparticles (NPs) have recently emerged as a new generation of nanoprobes for bioimaging.[12] For practical biomedical applications, highly emissive NPs are desirable to obtain high contrast imaging. Ideally, the most straightforward strategy to enhance fluorescence signals is to increase the number of encapsulated dye molecules in each NP. However, there are several inherent limitations that hamper full potential of conventional organic dye molecules as sensitive fluorescence probes. First, many conventional organic fluorophores have hydrophobic planar structures which show strong intermolecular π–π interactions to favor dye aggregation, leading to quenched fluorescence at high concentrations or in aggregates.[13] Second, the majority of commercial organic dyes suffers from severe "self-absorption" resulting from the small Stokes shift of less than 25 nm.[14] The poor separation between the absorption and emission spectra also hampers the use of optical filters to effectively block excitation light from reaching the fluorescence detector. Moreover, low resistance to photobleaching is another disadvantage of most organic dyes[15]

W. Qin, Dr. M. Li, Dr. Z. Yang, Prof. B. Z. Tang
Department of Chemistry
Institute for Advanced Study
Institute of Molecular Functional Materials
and Division of Biomedical Engineering
The Hong Kong University of Science & Technology (HKUST)
Clear Water Bay, Kowloon, Hong Kong, China
E-mail: tangbenz@ust.hk
Dr. K. Li, Prof. B. Liu
Institute of Materials Research and Engineering
3, Research Link, Singapore, 117602
E-mail: cheliub@nus.edu.sg
G. Feng, Prof. B. Liu
Department of Chemical and Biomolecular Engineering
National University of Singapore
4 Engineering Drive 4, Singapore, 117576
W. Qin, Dr. M. Li, Dr. Z. Yang, Prof. B. Z. Tang
HKUST-Shenzhen Research Institute
No. 9 Yuexing 1st RD, South Area, Hi-tech Park
Nanshan, Shenzhen, 518057, China
Prof. B. Z. Tang
Guangdong Innovative Research Team
SCUT-HKUST Joint Research Laboratory
State Key Laboratory of Luminescent Materials and Devices
South China University of Technology (SCUT)
Guangzhou, 51640, China

DOI: 10.1002/adfm.201302114

due to photon-induced chemical damage, which obviously compromises image quality. The combined drawbacks make many conventional dyes not ideal for fabrication of nanoparticle based probes.

Recently, we have successfully developed a novel class of organic luminogens with an extraordinary aggregation-induced emission (AIE) feature.[16] These luminogens, for example, tetraphenylethene (TPE), are nonemissive in dilute solutions but are induced to luminesce intensely when aggregated through a mechanism of restriction of intramolecular rotation (RIR).[17] Previous studies revealed that AIE luminogens are ideal candidates for the fabrication of fluorescent NPs due to their efficient emission in aggregate state.[18] In addition, surface functionalization of the NPs[19] with cell penetrating peptides, such as Tat,[20] yielded surface functionalized nanoparticles that can be internalized easily by cells and thus further improve the sensitivity of fluorescence imaging.[21]

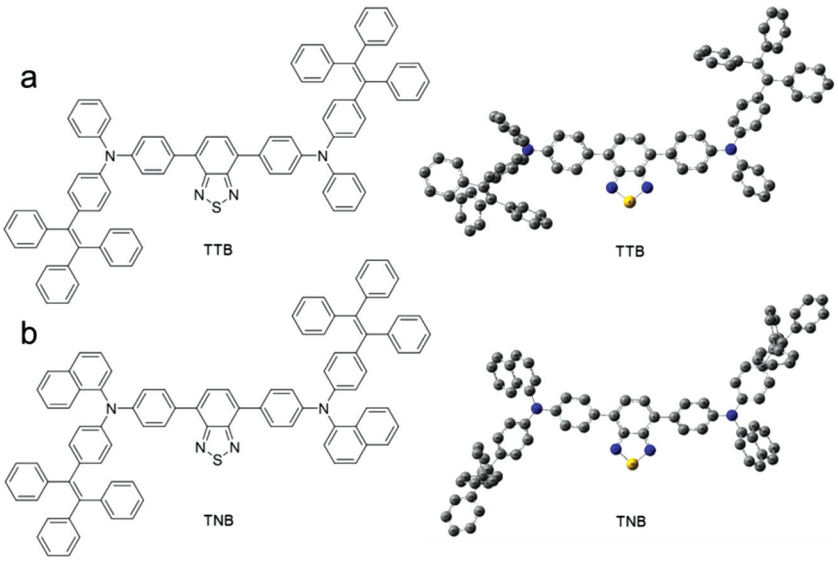

Figure 1. Chemical structures and molecular geometries of a) TTB and b) TNB; the molecular geometries were optimized by the DFT calculations using B3LYP/6-31G(d) basis set in Gaussian 03 program; hydrogen atoms were omitted for clarity.

To further fine-tune the emission wavelength and improve the fluorescence quantum yield of the nanoparticles, we report the synthesis of two orange-red emissive AIE-active compounds, TPE-TPA-BTD (TTB) and TPE-NPA-BTD (TNB), and the fabrication of their AIE dots for in vitro long-term cell tracing applications. Through conjugation with cysteine on C-terminus of modified Tat peptide(YGRKKRRQRRRC), the Tat functionalized AIE dots show high cellular internalization efficiency. The performances of the Tat-AIE dots in the in vitro studies were compared with those of commercially available QDs of Qtracker 585 under similar experimental conditions. It was found that the Tat-AIE dots could efficiently trace MCF-7 breast cancer cells as long as 5 days in vitro, which outperform their counterparts of commercial Qtracker 585 (1–2 days). Moreover, the first demonstration of AIE dots for intranuclear localization in live cells will provide a promising platform for intranuclear fluorescence imaging and future drug delivery. The excellent performance of the AIE dots sheds light on tracking and monitoring cells for cancer research and other cell-based therapies.

2. Results and Discussion

2.1. Synthesis and Characterization of TTB and TNB

The target molecules shown in **Figure 1** were synthesized according to **Scheme 1**. The key intermediate 4,7-bis(4-bromophenyl)-2,1,3-benzothiadiazole (**5**) was prepared from o-phenylenediamine (**1**) according to the previous report.[22] The reaction between intermediate **5** and aryl amines in the presence of palladium catalyst under basic conditions led to the products with >70% yields. The purified products were characterized by standard spectroscopic techniques, and the data indicate the right chemical structures with high purity. Detailed data are reported in the Experimental Section and the mass spectra of TTB and TNB are shown in Figures S1,S2 (Supporting Information). Both TTB and TNB possess good solubility in common organic solvents, such as tetrahydrofuran (THF), toluene, dichloromethane and chloroform, but are insoluble in water.

2.2. Optical Properties of AIE Luminogens

The compounds of TTB and TNB are comprised of arylamines as the electron donor (D), benzothiadiazole core as the electron acceptor (A) and TPE as iconic AIE unit. The D–A system is designed for obtaining fluorophores with long wavelength absorption and emission. The molecular fusion of the D–A system and TPE groups is expected to generate new AIE-active fluorogens with extended electronic conjugation. The absorption spectra of TTB and TNB in THF are peaked at 471 and 470 nm, respectively, indicative of very similar conjugation length of the two molecules (**Table 1**). Density functional theory calculations of the TTB and TNB were carried out using a suite of Gaussian 03 program in order to understand their properties at the molecular level. The nonlocal density functional of B3LYP with 6-31G(d) basis sets was used for the calculation. The optimized molecular geometries are shown in Figure 1, which adopt propeller-like conformations. The torsion angles between the central benzothiadiazole plane and their adjacent phenyl rings are ≈35° for both molecules (Tables S1,S2, Supporting Information). In the TPE part of TTB or TNB, the dihedral angles between any phenyl ring and the central double bond are ≈50°. The dihedral angles between any two phenyl rings of the arylamines in TTB are from ≈66° to ≈71° (Table S1, Supporting Information). However, the two dihedral angles of aromatic rings of arylamines in TNB are ≈82° (Table S2, Supporting Information). The nearly perpendicular conformations

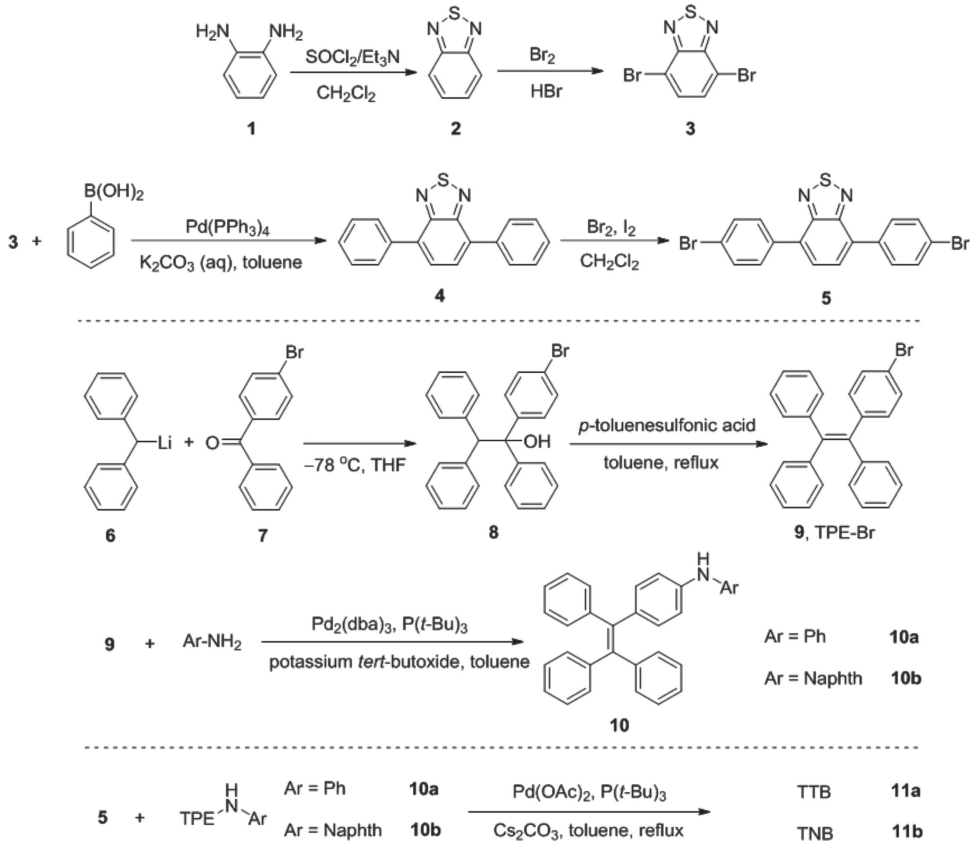

Scheme 1. Synthetic routes to TTB and TNB.

of TNB should disfavor close molecular packing in the solid state, leading to brighter fluorescence than that of TTB in condensed phase. In terms of the electronic structures, the lowest unoccupied molecular orbitals (LUMOs) of both molecules are dominated by the orbitals from the benzothiadiazole core. While the electron clouds of the highest occupied molecular orbitals (HOMOs) are mainly located on both the arylamine unit and benzothiadiazole core (Figure S3, Supporting Information). The difference in electron cloud distribution shows intrinsic intramolecular charge transfer (ICT) property, which is beneficial to red-shifted emission spectra.

The photoluminescence (PL) spectra of TTB and TNB were studied in THF/water mixtures with different water fractions (f_w), which is able to fine-tune the solvent polarity and the extent of solute aggregation (**Figure 2**). The pure THF solution of TTB emits orange-red light with an emission maximum at 616 nm. With gradual addition of water into THF ($f_w \leq 40\%$), the emission of TTB is weakened and is bathochromically shifted from 616 to 624 nm, possibly due to the increase in solvent polarity and hence the transformation to the twisted intramolecular charge transfer (TICT) state. The light emission is invigorated from $f_w \approx 50\%$ and is intensified with a further increase in f_w, indicating that TTB molecules form nanoaggregates due to the poor solubility. In the aqueous mixture with f_w of 90%, the emission of TTB is hypsochromically shifted to 609 nm. These data confirm that TTB is a luminogen with both TICT and AIE features. TNB shows a similar behavior (Figure 2c,d). In pure THF solution, the orange-red emission appears at 613 nm. Upon addition of water ($f_w \leq 40\%$), the emission is weakened and red-shifted. Whereas in the aqueous mixtures with "large"

Table 1. Optical Properties of TTB and TNB.

			λ_{em} (nm)[c]		
	λ_{ab} (nm)[a]	E_g (eV)[b]	soln	aggr	film ($\Phi_{F,f}$)[d]
TTB	471	2.26(2.45)	616	609	617 (48.8%)
TNB	470	2.27(2.48)	613	604	617 (63.0%)

[a]Absorption maximum (λ_{ab}) in THF; [b]HOMO–LUMO band gap (E_g) calculated from the onset of the absorption spectrum, HOMO is the highest occupied molecular orbital, LUMO is the lowest unoccupied molecular orbital. The values in the parentheses are derived from theoretical DFT calculations; [c]Emission maximum (λ_{em}) in THF solutions (soln, 10 μM), THF/water mixtures (aggr; 1:9 v/v; 10 μM), and solid thin films spin-coated from THF solution. [d]$\Phi_{F,f}$ is the fluorescence quantum efficiency in thin film state measured by a calibrated integrating sphere.

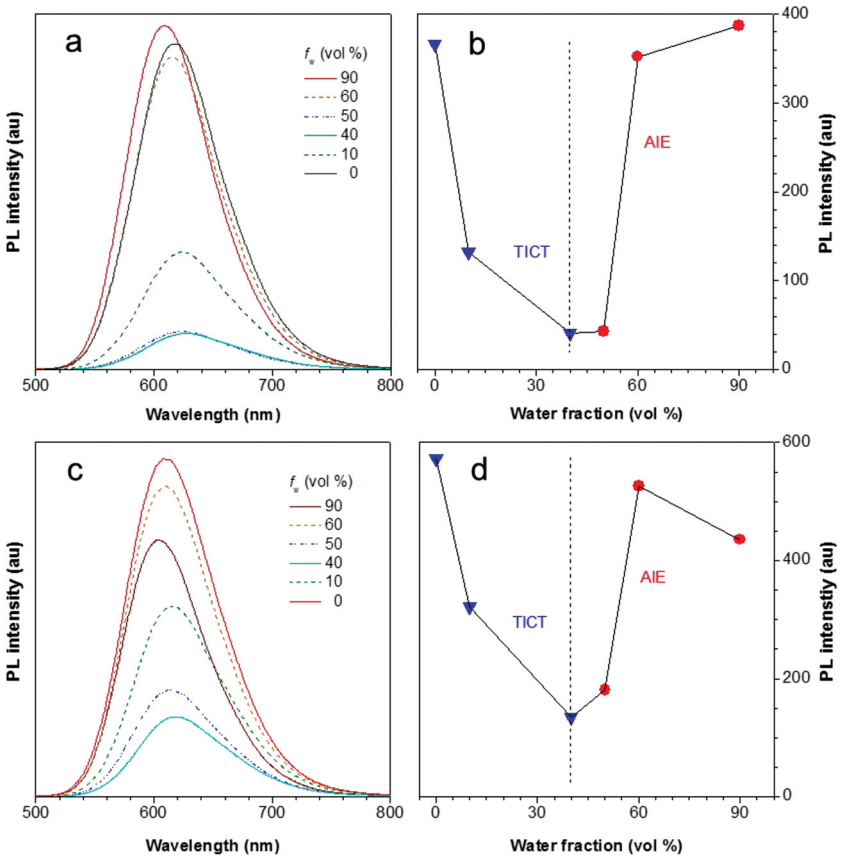

Figure 2. PL spectra of a) TTB and c) TNB in THF/water mixtures with different water fractions (f_w). Plot of peak intensity versus water fraction in the THF-water mixture of b) TTB and d) TNB. Concentration: 10 μM; excitation wavelength: 470 nm.

amounts of water (f_w > 40%), the emission is intensified and blue-shifted to 604 nm with f_w of 90%. The quantum yields (Φ_F) of TTB and TNB in solid state reach 48.8 and 63.0%, respectively (Table 1), which make both molecules good candidates for fabrication of AIE dots for bioimaging applications.

2.3. Preparation and Characterization of Tat-AIE Dots

To facilitate further conjugation with biomolecules, the AIE dot with maleimide groups on the surface were fabricated through a modified nanoprecipitation method reported by our group (**Scheme 2**).[23] A mixture of 1,2-distearoyl-*sn*-glycero-3-phosphoethanolamine-*N*-[methoxy(polyethylene glycol)-2000] (DSPE-PEG2000) and 1,2-distearoyl-*sn*-glycero-3-phosphoethanolamine-*N*-[maleimide(polyethylene glycol)-2000] (DSPE-PEG_{2000}-Mal) was employed as the encapsulation matrix. In brief, a THF solution of TTB or TNB (1 mg), DSPE-PEG_{2000} (1 mg) and DSPE-PEG_{2000}-Mal (1 mg) were mixed with water under continuous sonication. During the process, the hydrophobic DSPE segments were embedded in the hydrophobic core consisting of AIE luminogens and the hydrophilic PEG-Mal chains extended in aqueous phase to afford surface maleimide groups. After THF removal, the water suspensions of TTB and TNB dots were further mixed with Tat peptide, HIV-1 Tat (47-57), which could facilitate dots to enter live cells. The obtained Tat-TTB and Tat-TNB dots have excellent colloidal stability in water as no obvious precipitation from the stock suspensions was observed after being stored at 4 °C for months.

The sizes of Tat-TTB and Tat-TNB dots were investigated by laser light scattering (LLS), suggesting that the volume average hydrodynamic diameters are ≈36 and 38 nm, respectively (**Figure 3**a,c). The morphology of Tat-AIE dots was further investigated using high-resolution transmission electron microscopy (HR-TEM), indicating that they are in spherical shape and the dark dots are due to the high electron density of AIE luminogens (Figure 3a,c). As shown in Figure 3b,d, Tat-TTB and Tat-TNB dots have the same absorption peaks at 480 nm. The emission maxima of Tat-TTB and Tat-TNB dots appear at 619 and 617 nm, respectively, with intense emission tails extending to 850 nm. It is noteworthy that the Stokes shifts of the AIE dots are larger than 130 nm, which greatly minimize the self-absorption effect universally observed in conventional organic dye molecules. The quantum yields of Tat-TTB and Tat-TNB dots in water are 55% and 67%, respectively, measured using 4-(dicyanomethylene)-2-methyl-6-(*p*-dimethylaminostyryl)-4*H*-pyran (DCM) in methanol as a standard (Φ_F = 43%). The high quantum yields of AIE dots are beneficial to high signal-to-noise ratios in cell imaging.

2.4. In Vitro Cell Imaging

The application of as-prepared Tat-AIE dots in cell imaging was studied by confocal laser scanning microscopy. In these experiments, MCF-7 breast cancer cells were incubated with 2 nM

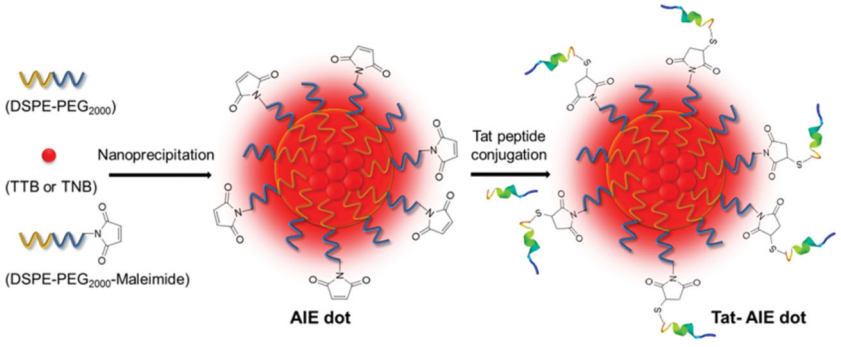

Scheme 2. Schematic illustration of the preparation of Tat-functionalized AIE dots.

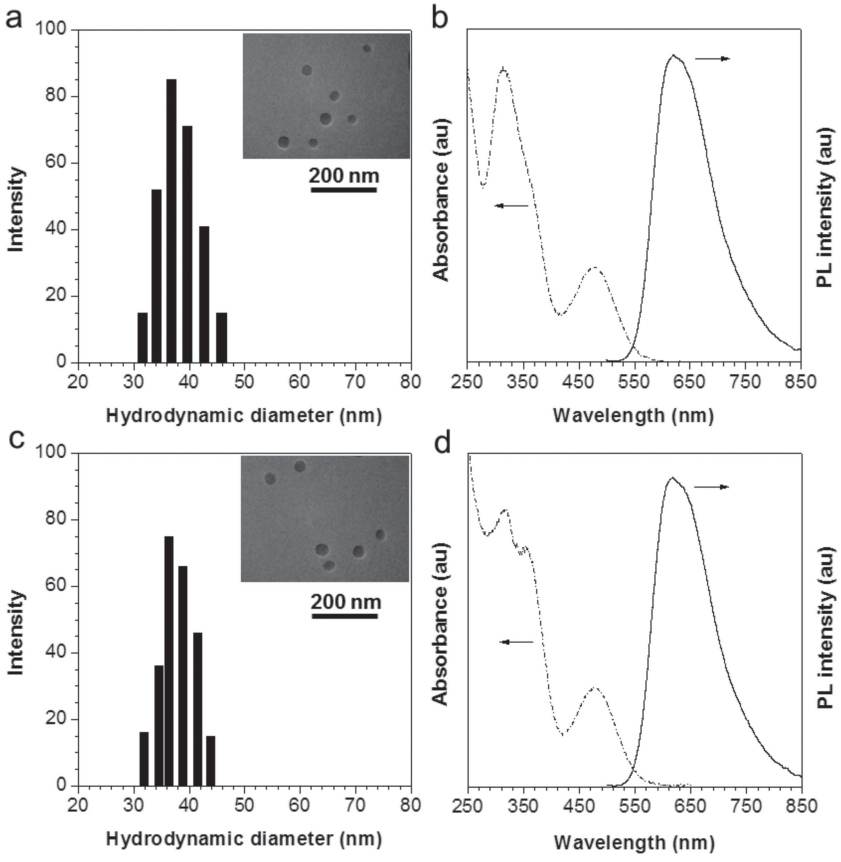

Figure 3. Particle size distributions studied by laser light scattering and HR-TEM images of a) Tat-TTB and c) Tat-TNB dots. Absorption and emission spectra of b) Tat-TTB and d) Tat-TNB dots suspended in water; λ_{ex} = 488 nm.

Tat-TTB or Tat-TNB suspensions for 6 h. The calculation of dot concentration is described in the Supporting Information. Hoechst 34580 was then used to stain the cell nuclei for 30 min before live cell imaging studies. The cellular uptake and localization of Tat-AIE dots in live MCF-7 cancer cells are shown in **Figure 4**. The images were taken upon excitation at 405 nm (1 mW) while 440–480 nm and 600–800 nm bandpass filters were adopted for simultaneous collection of fluorescence from Hoechst 34580 and Tat-AIE dots, respectively. It is obvious that abundant Tat-TTB dots (Figure 4a) and Tat-TNB dots (Figure 4e) localize in the cytoplasm and the perinuclear region. To a certain extent, some orange-red emission is also observed from the nuclei region (Figure **4c**,g), indicating that some AIE dots might locate in the cell nuclei. 3D sectional images of MCF-7 cancer cells (Figure **4d**,h) further reveal that the AIE dots are indeed located in the nuclei, possibly because some of them traverse the nuclear pore complex (NPC) to the nucleus by passive diffusion.[24]

To further investigate the importance of surface-conjugated Tat peptide in cellular imaging, TTB dots and TNB dots without functionalization with Tat were also incubated with MCF-7 cancer cells under the same experimental conditions. As shown in Figure S4 in the Supporting Information, the TTB and TNB dots are found randomly distributed in cell cytoplasm and no fluorescence from the dots can be detected in the nucleus region. Moreover, the fluorescence intensity from cell cytoplasm (Figure S4, Supporting Information) is much lower as compared to that in Figure 4. These results not only verify that Tat peptides can greatly enhance live cell internalization efficiency but also further confirm the vital role of Tat peptide functionalized on the surface of AIE dots in facilitating the intranuclear translocation.[25] Our findings are consistent with previously reported inorganic nanoparticles studies, which showed that gold[26] and silica[27] nanoparticles with diameters of <50 nm could penetrate cell nuclei after conjugation with Tat peptides. The first demonstration of AIE dots for intranuclear localization in live cells will provide a promising platform for intranuclear fluorescence imaging and future drug delivery.

2.5. Photostability and Cytotoxicity of AIE Dots

Figure 5a shows the fluorescence change of Tat-AIE dots and Qtracker 585 dots in cells upon continuous laser irradiation at 488 nm (2 mW) for 20 min. After irradiation, the Tat-AIE dots possess ≈94% of their initial fluorescence intensity, which is comparable to that of Qtracker 585 dots. Noteworthy is that the laser power employed is twice

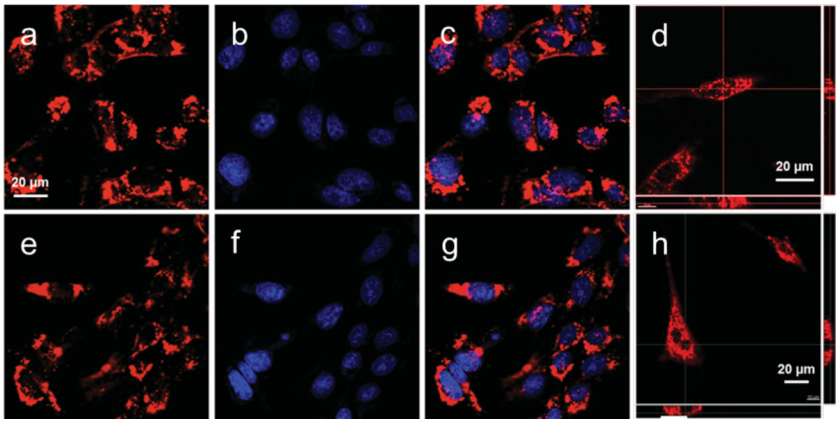

Figure 4. Confocal images of live MCF-7 breast cancer cells after incubation with 2 nM a) Tat-TTB and e) Tat-TNB dots for 6 h at 37 °C. b,f) The live cell nuclei were stained by Hoechst 34580 for 30 min. c,g) The corresponding overlay images. 3D sectional confocal images of MCF-7 breast cancer cells after incubation with 2 nM d) Tat-TTB and h) Tat-TNB dots for 6 h at 37 °C. The images (a–c,e–g) share the same scale bar.

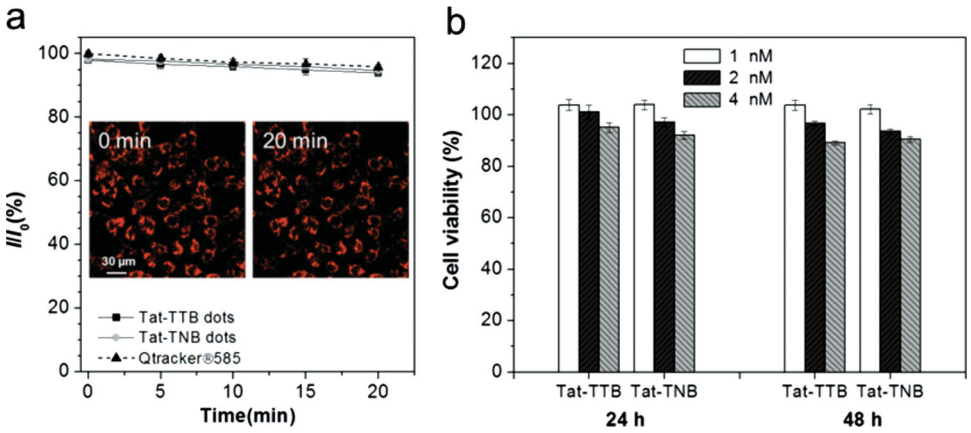

Figure 5. a) Photostability of Tat-TTB and Tat-TNB dots under continuous scanning at 488 nm (2 mW). Insets show confocal images of the Tat-TTB dot-stained cells before (0 min, left) and after the laser irradiation for 20 min (right). I_0 is the initial PL intensity, while I is that of the corresponding sample after a designated time interval. b) Cell viability of MCF-7 cells after incubation with 1, 2, and 4 nM Tat-TTB, Tat-TNB dots for 24 h, 48 h, respectively.

as high as that used in in vitro fluorescence imaging studies (1 mW). Unlike traditional organic dyes which suffer from severe photobleaching after several minutes of laser irradiation,[28] the AIE dots exhibit excellent photostability, which will greatly benefit their in vitro long-term cell tracing studies. The cytotoxicity of the AIE dots was evaluated by metabolic viability of MCF-7 breast cancer cells after incubation with the different concentration of dots. Figure 5b shows the cell viability after incubation with Tat-TTB and Tat-TNB dots at dot concentrations of 1, 2, and 4 nM for 24 and 48 h, respectively. Cell viabilities remain above 95% after being treated with 1 and 2 nM Tat-AIE dotswithin the tested periods of time. It still remains above 90% after being treated with 4 nM Tat-AIE dots even for 48 h, indicating low cytotoxicity of the AIE dots in the test, which is essential for long-term tracing applications.

2.6. In Vitro Cell Tracing

MCF-7 human breast cancer cells were chosen as a model to demonstrate the ability of Tat-AIE dots for in vitro cell tracing application. The MCF-7 cancer cells were first incubated with 2 nM Tat-AIE dots ovenight at 37 °C. The labeled cells were then subcultured for designated time intervals and the fluorescence profiles were recorded using flow cytometry by counting 10 000 events with 488 nm excitation and, 575/25 nm bandpass filter.

Figure 6a shows that the labeling rate of Tat-TTB dots towards MCF-7 cells is 99.8% on the 1st day and is above 93% on the 4th day. It remains above 86% on the 5th day as compared to the untreated cells, which is still higher than that of Qtracker 585-treated cells on the 1st day (84%). The labeling rate for Tat-TTB is 24.5% after continuous culture till the 9th day. Similarly, the labeling rate of Tat-TNB towards MCF-7 cells is 99.9% on the first day. It remains 94.9% on the 4th day and also above 86.0% at 5th day as compared to the untreated cells (Figure 6b). The labeling rate is 28.8% after continuous culture till 8th day. The gradually decreased fluorescence intensity in each single cell can be attributed to the continuous cell division while the internalized Tat-AIE dots are inherited by daughter cells. On the contrary, the initial labeling rate of Qtracker 585 is around 84.0% on the 1st day, and only 26.9% of Qtracker 585 -treated cells are labeled at the 5th day (Figure 6c). The results clearly indicate the superior cell tracing ability of Tat-AIE dots over Qtracker 585. These results were further confirmed by confocal images (**Figure 7**). Only very weak fluorescence is detectable in Qtracker 585-labeled cells while the Tat-AIE dot-labeled cells show high fluorescence signal on the 3rd day. The fluorescence of Qtracker 585 in MCF-7 cells fades out on the 5th day, while the signal of Tat-AIE dots can still be collected on the 7th day. The fluorescence signal in Figure 7 is from the Tat-AIE dots since cell autofluorescence is not detectable under the same experimental conditions (Figure S5, Supporting Information).

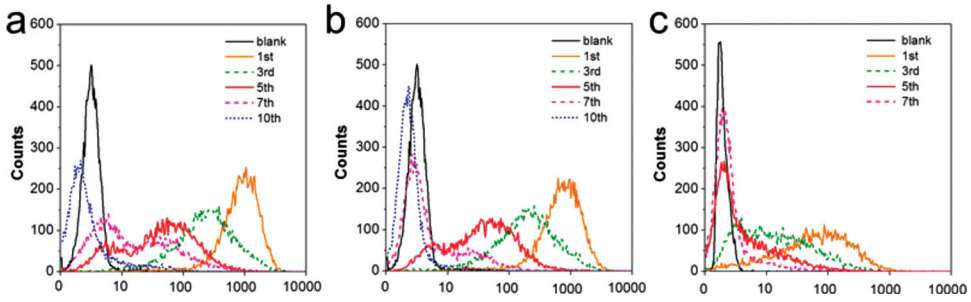

Figure 6. Flow cytometry histograms of MCF-7 breast cancer cells after overnight incubation with 2 nM a) Tat-TTB, b) Tat-TNB dots, and c) Qtracker 585 dots at 37 °C and then subcultured for designated time intervals (day). The untreated MCF-7 cells were used as the control (blank).

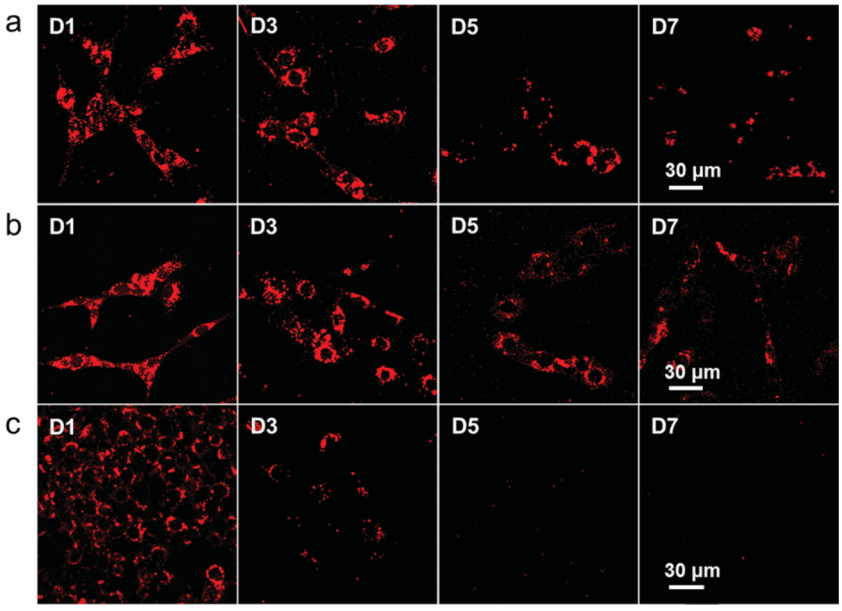

Figure 7. CLSM images of MCF-7 on designated days after the overnight incubation of a) Tat-TTB dots, b) Tat-TNB dots, and c) Qtracker 585 dots at a concentration of 2 nM. The confocal images were taken under excitation at 488 nm (≈1 mW) with signal collected above 505 nm.

As Qtracker labeling kits are the most commonly used long-term fluorescent tracing probes, the Tat-AIE dots can serve as an ultrabright and ultrastable probe in long-term cell tracing and imaging applications.

3. Conclusions

In summary, we have synthesized two AIE luminogens (TTB and TNB), fabricated the corresponding functionalized AIE dots and explored their in vitro bioimaging applications. The two AIE luminogens possess both TICT and AIE features. The formulated Tat-TNB dots exhibit higher emission efficiency compared to Tat-TTB dots, while the two AIE dots have similar performance in imaging: both AIE dots show high emission efficiency, large Stokes shift, good biocompatibility, and high photobleaching resistance, exhibiting superior performance in long-term cell tracing as compared to that for commercial QD-based cell tracing probes. Further efforts will be made to control the size and modify the surface of AIE dots to improve their internalization efficiency for cellular nucleus imaging.

4. Experimental Section

Materials: 4,7-Dibromo-2,1,3-benzothiadiazole 3,[29] 4,7-bis(4-bromophenyl)-2,1,3-benzothiadiazole 5,[22] TPE derivative, 10,[11] were prepared according to the literature methods. THF was distilled from sodium benzophenone ketyl under dry nitrogen immediately prior to use. All the chemicals and other regents were purchased from Aldrich and used as received without further purification. All reactions and manipulations were carried out under nitrogen gas with the use of standard inert atmosphere. 1,2-Distearoyl-*sn*-glycero-3-phosphoethanolamine-*N*-[methoxy(polyethylene glycol)-2000] (DSPE-PEG_{2000}) was a gift from Lipoid GmbH (Ludwigshafen, Germany).1,2-distearoyl-*sn*-glycero-3-phosphoethanolamine-*N*-[maleimide(polyethylene glycol)-2000] (DSPE-PEG_{2000}-Mal) was a commercial product of Avanti Polar Lipids, Inc. Dulbecco's Modified Eagle Medium (DMEM), and 3-(4,5-dimethylthiazol-2-yl)-2,5-diphenyl tetrazolium bromide (MTT) were purchased from Sigma-Aldrich. Hoechst 34580, penicillin-streptomycin solution, fetal bovine serum (FBS) and trypsin-EDTA solution were purchased from Life Technologies, Singapore. HIV-1 Tat (47-57) derived from transactivator of transcription proteins was modified with cysteine on C-terminus (YGRKKRRQRRRC), which was a commercial product customized by GenicBio (Shanghai, China). Milli-Q water was supplied by Milli-Q Plus System (Millipore Corporation, Breford, USA). MCF-7 breast cancer cells were provided by American Type Culture Collection.

Characterization: ^{1}H- and ^{13}C-NMR spectra were measured on a Bruker AV 300 or 400 spectrometer in $CDCl_3$ or CD_2Cl_2 using tetramethylsilane (TMS; $\delta = 0$) as internal reference. The UV-vis spectra were measured on a Shimadzu UV-1700 spectrometer. The fluorescence spectra of dots were recorded using a fluorometer (LS-55, Perkin Elmer, USA). High resolution mass spectra (HRMS) were recorded on a GCT premier CAB048 mass spectrometer operating in MALDI-TOF mode. Elemental analysis was performed on a ThermoFinnigan Flash EA1112. Fluorescence quantum efficiencies of the organic compounds in films were measured using a calibrated integrating sphere. The average particle size and size distribution were determined by laser light scattering with a particle size analyzer (90 Plus, Brookhaven Instruments Co. USA) at a fixed angle of 90° at 24 °C. The morphology of dots was studied by high-resolution transmission electron microscope (HR-TEM, JEM-2010F, JEOL, Japan).

Preparation of TTB and TNB Nanoaggregates: Stock solutions of the compounds in THF with a concentration of 10^{-4} M were prepared. Aliquots of the stock solution were transferred to 10 mL volumetric flasks. After appropriate amounts of THF were added, water was added dropwise under vigorous stirring to furnish 10^{-5} M solutions with different water contents (0–90 vol%). The PL measurements of the resultant solutions were then performed immediately.

Preparation of TTB: A mixture of compound 5 (223 mg, 0.5 mmol), *N*-(4-(1,2,2-triphenylvinyl)phenyl)benzenamine (10a) (634 mg, 1.5 mmol), Cs_2CO_3 (1.14 g, 3.5 mmol), $Pd(OAc)_2$ (11.2 mg, 0.05 mmol), P(*t*-Bu)$_3$ (30.3 mg, 0.15 mmol) and toluene (40 mL) was heated at 40 °C for 2 h. And then the reaction mixture heated at 110 °C for 24 h. After the mixture was cooled to room temperature, water (30 mL) and chloroform (300 mL) were added. An organic layer was separated and washed with brine, dried over anhydrous $MgSO_4$, and evaporated to dryness under reduced pressure. The crude product was purified by column chromatography on silica gel using hexane/toluene as eluent, affording orange red solid in 71% yield (401 mg). ^{1}H NMR (400 MHz, CD_2Cl_2), δ (TMS, ppm): 7.87 (d, J = 8.8 Hz, 4H), 7.74 (s, 2H), 7.27 (t, J = 8.0 Hz, 4H), 7.16–7.02 (m, 40H), 6.93–6.91 (m, 4H), 6.88–6.86 (m, 4H). ^{13}C NMR (75 MHz, $CDCl_3$), δ (TMS, ppm): 154.30, 147.88, 147.41, 145.74, 144.15, 143.87, 143.70, 140.86, 140.80, 138.79, 132.44, 132.29, 131.53, 131.50, 131.17, 129.97, 129.42, 127.82, 127.76, 127.56, 126.61, 126.56, 126.49, 125.20, 123.75, 123.42, 123.18. HRMS (MALDI-TOF, m/z): [M$^+$] calcd for $C_{82}H_{58}N_4S$: 1130. 4382; found, 1130.4374. Anal. calcd for $C_{82}H_{58}N_4S$: C, 87.05; H, 5.17; N, 4.95; S, 2.83. found: C, 86.81; H, 5.13; N, 4.92.

*Preparation of*10b: The compound was prepared from compound 9 and 1-Naphthylamine according to the reported methods.[11]^{1}H NMR (400 MHz, $CDCl_3$), δ (TMS, ppm): 7.98–7.96 (m, 1H), 7.86–7.83 (m, 1H), 7.55–7.44 (m, 3H), 7.39–7.35 (m, 2H), 7.18–7.01 (m, 15H), 6.91 (d, J = 8.4 Hz, 2H), 6.77 (d, J = 8.4 Hz, 2H). ^{13}C NMR (75 MHz, $CDCl_3$), δ (TMS, ppm):144.34, 144.20, 144.12, 142.89, 140.90, 140.00, 138.53,

136.07, 134.79, 132.58, 131.61, 131.52, 128.66, 127.85, 127.73, 127.72, 127.54, 126.48, 126.37, 126.31, 126.20, 126.06, 125.71, 122.89, 121.76, 116.59, 115.62. HRMS (MALDI-TOF, *m/z*): [M$^+$] calcd for $C_{36}H_{27}N$, 473.2143; found 473.1956.

Preparation of TNB: The compound was prepared from compound 5 (223 mg, 0.5 mmol), *N*-(4-(1,2,2-triphenylvinyl)phenyl)naphthalen-1-amine (10b) (710 mg, 1.5 mmol), Cs_2CO_3 (1.14 g, 3.5 mmol), $Pd(OAc)_2$ (11.2 mg, 0.05 mmol), and P(*t*-Bu)$_3$ (30.3 mg, 0.15 mmol), following the same procedure described above, affording orange red solid in 78% yield (480 mg). ^{1}H NMR (300 MHz, $CDCl_3$), δ (TMS, ppm): 7.92–7.87 (t, 4H), 7.77 (t, J = 8.4 Hz, 6H), 7.64 (s, 2H), 7.46 (t, J = 8.0 Hz, 4H), 7.41–7.35 (m, 4H), 7.14–6.99 (m, 34H), 6.86 (s, 8H). ^{13}C NMR (75 MHz, $CDCl_3$), δ (TMS, ppm):154.28, 148.48, 146.22, 144.13, 143.96, 143.76, 143.13, 140.81, 140.60, 137.83, 135.43, 132.32, 132.16, 131.50, 131.34, 130.27, 129.87, 128.55, 127.76, 127.73, 127.51, 127.38, 126.84, 126.53, 126.47, 126.41, 126.29, 124.44, 121.67, 121.11. HRMS (MALDI-TOF, *m/z*): [M$^+$] calcd for $C_{90}H_{62}N_4S$, 1230.4695; found, 1230.5199). Anal. calcd for $C_{90}H_{62}N_4S$: C, 87.77; H, 5.07; N, 4.55; S, 2.60. found: C, 87.91; H, 5.15; N, 4.62.

Synthesis of Tat Peptide-Functionalized AIE Dots: Two AIE chromophores were used in synthesis of Tat peptide-functionalized AIE dots. TTB (1 mg), DSPE-PEG$_{2000}$ (1 mg) and DSPE-PEG$_{2000}$-Mal (1 mg) were dissolved in 1 mL of THF solution, followed by mixing with 9 mL of water. The mixture was then sonicated for 60 seconds using a microtip probe sonicator at 15 W output (XL2000, Misonix Incorporated, NY). After filtration using a 0.2 μm syringe driven filter, the suspension was stirred vigorously at room temperature overnight to yield TTB dots in water (8 mL). The AIE dot suspension (2 mL) was further mixed with the modified HIV1-Tat peptide (5×10^{-5} M). After reaction overnight at room temperature, the solution was dialysed against MilliQ water for 2 days to eliminate the excess peptides. The Tat-TTB dots were collected for further use. TNB was also used to fabricate Tat-TNB dots following the same experimental procedures.

Cell Culture: MCF-7 breast cancer cells were cultured in DMEM containing 10% fetal bovine serum and 1% penicillin streptomycin at 37 °C in a humidified environment containing 5% CO_2. Before experiment, the cells were pre-cultured until confluence was reached.

In Vitro Cell Imaging: MCF-7 breast cancer cells were cultured in 8-well confocal chambers (Costar, IL, USA) to achieve 80% confluence. The medium was then removed and cell monolayer was washed twice with 1× PBS buffer. Tat-TTB dots or Tat-TNB dots in DMEM (2 nM) were then added to the sample wells. After 6 h incubation at 37 °C, the cells were washed twice with 1× PBS buffer and freshly prepared Hoechst 34580 solution in DMEM (1 μg mL^{-1}) was added into the wells for further 30 min incubation. The cells were then washed twice with 1× PBS buffer. After addition of fresh DMEM, the cells were immediately imaged by Leica TCS SP 5X. The laser at 405 nm (1 mW) was used to obtain the one-photon excited fluorescence images with 440–480 nm and 600–800 nm bandpass filters for simultaneous collection of fluorescence from Hoechst 34580 and Tat-AIE dots, respectively.

Cytotoxicity of AIE Dots and Tat-AIE Dots: The metabolic viability of MCF-7 breast cancer cells were evaluated using methylthiazolyldiphenyltetrazolium bromide (MTT) assays. MCF-7 breast cancer cells were seeded in 96-well plates (Costar, IL, USA) at an intensity of 6×10^4 cells mL^{-1}, respectively. After 24 h incubation, the old medium was replaced by Tat-AIE dot suspension at concentrations of 1, 2, and 4 nM, and the cells were then incubated for 24 h and 48 h, respectively. The wells were then washed twice with 1× PBS buffer and 100 μL of freshly prepared MTT (0.5 mg mL^{-1}) solution in culture medium was added into each well. The MTT medium solution was carefully removed after 3 h incubation. Filtered DMSO (100 μL) was then added into each well and the plate was gently shaken for 10 min to dissolve all the precipitates formed. The absorbance of MTT at 570 nm was monitored by the microplate reader (Genios Tecan). Cell metabolic viability was expressed by the ratio of the absorbance of the cells incubated with Tat-AIE dot suspension to that of the cells incubated with culture medium only.

In Vitro Cell Tracing: MCF-7 breast cancer cells were cultured in 6-well plates (Costar, IL, USA) to achieve 80% confluence. After medium removal and washing with 1× PBS buffer, 2 nM Tat-AIE dots or Qtracker 585 in DMEM were then added to the wells. After overnight incubation at 37 °C, the cells were washed twice with 1× PBS buffer and detached by 1× tripsin and resuspended in culture medium. Upon dilution, the cells were subcultured in 6-well plates for 1 to 10 day regeneration, respectively. After designated time points, the cells were washed twice with 1× PBS buffer and then trypsinized to suspend in 1× PBS buffer. The fluorescence intensities of cells were then analyzed by flow cytometry measurements using Cyan-LX (DakoCytomation) and the histogram of each sample was obtained by counting 10 000 events (λ_{ex} = 488 nm, 575/25 nm bandpass filter). For confocal image studies, the cells were first labeled by 2 nM Tat-AIE dots or Qtracker 585. The labeled cells were then washed twice with 1× PBS buffer and trypsinized to suspend in culture medium. The cells were then diluted and subcultured in 6-well plates containing cell culture coverslips for designated passages. Upon reaching designated time points, the cells were washed twice with 1× PBS buffer and then fixed by 75% ethanol for 20 min. The coverslips were sealed with mounting medium and used for confocal imaging.

Supporting Information

Supporting Information is available from the Wiley Online Library or from the author.

Acknowledgment

W.Q. and K.L. contributed equally to this work. This work was partially supported by the National Basic Research Program of China (973 Program, 2013CB834701), the RPC and SRFI Grants of HKUST (RPC11SC09 and SRFI11SC03PG), the Research Grants Council of Hong Kong (HKUST2/CRF/10 and N_HKUST620/11), and the University Grants Committee of Hong Kong (AoE/P-03/08), and Singapore Institute of Materials Research and Engineering (IMRE/13-8P1104; IMRE/13-1P0909), and National Research Foundation (R279-000-390-281). The authors thank the support of the Guangdong innovative Research Team Program (201101C0105067115). The authors also thank Professor Kam Sing Wong in Department of Physics, HKUST for the measurement of fluorescence quantum yields of solid powder samples.

Received: June 21, 2013
Revised: July 12, 2013
Published online: September 6, 2013

[1] a) B. N. G. Giepmans, S. R. Adams, M. H. Ellisman, R. Y. Tsien, *Science* **2006**, *312*, 217; b) T. Terai, T. Nagano, *Curr. Opin. Chem. Biol.* **2008**, *12*, 515.
[2] a) D. W. Domaille, E. L. Que, C. J. Chang, *Nat. Chem. Biol.* **2008**, *4*, 168; b) R. Y. Tsien, *Angew. Chem. Int. Edit.* **2009**, *48*, 5612; c) M. Y. Hu, L. Li, H. Wu, Y. Su, P. Y. Yang, M. Uttamchandani, Q. H. Xu, S. Q. Yao, *J. Am. Chem. Soc.* **2011**, *133*, 12009.
[3] a) S. Wang, T. Hazelrigg, *Nature* **1994**, *369*, 400; b) C. J. Daly, J. C. McGrath, *Pharmacol. Ther.* **2003**, *100*, 101.
[4] a) F. Q. Chen, D. Gerion, *Nano Lett.* **2004**, *4*, 1827; b) J. K. Jaiswal, E. R. Goldman, H. Mattoussi, S. M. Simon, *Nat. Methods* **2004**, *1*, 73; c) L. S. Shah, P. A. Clark, E. K. Moioli, M. A. Stroscio, J. J. Mao, *Nano Lett.* **2007**, *7*, 3071.
[5] Y. G. Meng, J. Liang, W. L. Wong, V. Chisholm, *Gene* **2000**, *242*, 201.
[6] E. Dellambra, G. Pellegrini, L. Guerra, G. Ferrari, G. Zambruno, F. Mavilio, M. De Luca, *Hum. Gene Ther.* **2000**, *11*, 2283.
[7] a) X. H. Gao, Y. Y. Cui, R. M. Levenson, L. W. K. Chung, S. M. Nie, *Nat. Biotechnol.* **2004**, *22*, 969; b) X. Michalet, F. F. Pinaud,

L. A. Bentolila, J. M. Tsay, S. Doose, J. J. Li, G. Sundaresan, A. M. Wu, S. S. Gambhir, S. Weiss, *Science* **2005**, *307*, 538.

[8] A. M. Smith, H. W. Duan, A. M. Mohs, S. M. Nie, *Adv. Drug Delivery Rev.* **2008**, *60*, 1226.

[9] a) J. A. Kloepfer, R. E. Mielke, M. S. Wong, K. H. Nealson, G. Stucky, J. L. Nadeau, *Appl. Environ. Microb.* **2003**, *69*, 4205; b) A. M. Derfus, W. C. W. Chan, S. N. Bhatia, *Nano Lett.* **2004**, *4*, 11; c) S. J. Cho, D. Maysinger, M. Jain, B. Roder, S. Hackbarth, F. M. Winnik, *Langmuir.* **2007**, *23*, 1974.

[10] a) C. Kirchner, T. Liedl, S. Kudera, T. Pellegrino, A. M. Javier, H. E. Gaub, S. Stolzle, N. Fertig, W. J. Parak, *Nano Lett.* **2005**, *5*, 331; b) J. F. Weng, J. C. Ren, *Curr. Med. Chem.* **2006**, *13*, 897.

[11] K. Li, W. Qin, D. Ding, N. Tomczak, J. Geng, R. Liu, J. Liu, X. Zhang, H. Liu, B. Liu, B. Z. Tang, *Sci. Rep.* **2013**, *3*, 1150.

[12] a) A. Palma, L. A. Alvarez, D. Scholz, D. O. Frimannsson, M. Grossi, S. J. Quinn, D. F. O'Shea, *J. Am. Chem. Soc.* **2011**, *133*, 19618; b) A. Wagh, S. Y. Qian, B. Law, *Bioconjugate. Chem.* **2012**, *23*, 981.

[13] a) I. B. Berlman, *Handbook of Fluorescence Spectra of Aromatic Molecules*, 2nd ed., Academic Press, New York **1971**; b) M. Shimizu, T. Hiyama, *Chem. Asian J.* **2010**, *5*, 1516.

[14] a) C. A. Bertolino, G. Caputo, C. Barolo, G. Viscardi, S. Coluccia, *J. Fluoresc.* **2006**, *16*, 221; b) W. Y. Lin, L. Yuan, Z. M. Cao, Y. M. Feng, J. Z. Song, *Angew. Chem. Int. Edit.* **2010**, *49*, 375.

[15] a) L. L. Song, E. J. Hennink, I. T. Young, H. J. Tanke, *Biophys. J.* **1995**, *68*, 2588; b) C. Eggeling, J. Widengren, R. Rigler, C. A. M. Seidel, *Anal. Chem.* **1998**, *70*, 2651; c) U. Resch-Genger, M. Grabolle, S. Cavaliere-Jaricot, R. Nitschke, T. Nann, *Nat. Methods* **2008**, *5*, 763.

[16] Y. N. Hong, J. W. Y. Lam, B. Z. Tang, *Chem. Soc. Rev.* **2011**, *40*, 5361.

[17] Y. N. Hong, J. W. Y. Lam, B. Z. Tang, *Chem. Commun.* **2009**, 4332.

[18] a) W. Z. Yuan, P. Lu, S. M. Chen, J. W. Y. Lam, Z. M. Wang, Y. Liu, H. S. Kwok, Y. G. Ma, B. Z. Tang, *Adv. Mater.* **2010**, *22*, 2159; b) Z. Zhao, S. Chen, X. Shen, F. Mahtab, Y. Yu, P. Lu, J. W. Y. Lam, H. S. Kwok, B. Z. Tang, *Chem. Commun.* **2010**, *46*, 686.

[19] M. Li, J. W. Y. Lam, F. Mahtab, S. J. Chen, W. J. Zhang, Y. N. Hong, J. Xiong, Q. C. Zheng, B. Z. Tang, *J. Mater. Chem. B* **2013**, *1*, 676.

[20] L. N. Patel, J. L. Zaro, W. C. Shen, *Pharmaceut. Res.* **2007**, *24*, 1977.

[21] V. P. Torchilin, *Adv. Drug Delivery Rev.* **2008**, *60*, 548.

[22] J. Liu, L. J. Bu, J. P. Dong, Q. G. Zhou, Y. H. Geng, D. G. Ma, L. X. Wang, X. B. Jing, F. S. Wang, *J. Mater. Chem.* **2007**, *17*, 2832.

[23] K. Li, Y. Jiang, D. Ding, X. Zhang, Y. Liu, J. Hua, S.-S. Feng, B. Liu, *Chem. Commun.* **2011**, *47*, 7323.

[24] C. W. Pouton, K. M. Wagstaff, D. M. Roth, G. W. Moseley, D. A. Jans, *Adv. Drug Delivery Rev.* **2007**, *59*, 698.

[25] a) S. Nakielny, G. Dreyfuss, *Cell* **1999**, *99*, 677; b) F. Alber, S. Dokudovskaya, L. M. Veenhoff, W. H. Zhang, J. Kipper, D. Devos, A. Suprapto, O. Karni-Schmidt, R. Williams, B. T. Chait, A. Sali, M. P. Rout, *Nature* **2007**, *450*, 695.

[26] N. Pante, M. Kann, *Mol. Biol. Cell* **2002**, *13*, 425.

[27] L. M. Pan, Q. J. He, J. N. Liu, Y. Chen, M. Ma, L. L. Zhang, J. L. Shi, *J. Am. Chem. Soc.* **2012**, *134*, 5722.

[28] a) H. Giloh, J. W. Sedat, *Science* **1982**, *217*, 1252; b) W. Qin, D. Ding, J. Z. Liu, W. Z. Yuan, Y. Hu, B. Liu, B. Z. Tang, *Adv. Funct. Mater.* **2012**, *22*, 771.

[29] B. A. D. Neto, A. S. A. Lopes, G. Ebeling, R. S. Goncalves, V. E. U. Costa, F. H. Quina, J. Dupont, *Tetrahedron* **2005**, *61*, 10975.